

## Analysis of ferroelectric ceramic fabricated by binder jetting technology

Sara M. Gaytan<sup>1</sup>, Monica Cadena<sup>1</sup>, Mayela Aldaz<sup>1</sup>, Edward Herderick<sup>2</sup>, Francisco Medina<sup>1</sup>, Ryan Wicker<sup>1</sup>

<sup>1</sup>W.M. Keck Center for 3D Innovation, The University of Texas at El Paso, El Paso, TX

<sup>2</sup>Materials Group, EWI, Columbus, OH

Accepted August 16th 2013

### Abstract

The M-Lab system from ExOne was used to fabricate 3D structures of BaTiO<sub>3</sub> ceramic with applications that include dielectric capacitors, sensors, and integrated circuits. For this project, layer thicknesses of 15 and 30 μm and various percentages of binder saturation were used to fabricate components from powder. An organic binding agent was utilized during the printing process and later burned out at ~600°C prior to sintering. Multiple building parameters and sintering profiles were analyzed and compared in an attempt to obtain dense parts while examining shrinkage percentage variations.

### Introduction

Barium titanate IV [BaTiO<sub>3</sub>] (BTO) applications range from embedded capacitance in printed circuit board to piezoelectric devices like sensors, heaters and transducers (*Buscaglia, et al.* 2004) (*Maison, et al.* 2001). Other applications include semiconductors with positive temperature coefficient of resistivity (PTCR) (*Chatterjee, Stojanovic and Maiti* 2003), dynamic access memories (DRAM), and IR sensors (*Sahoo, et al.* 2007). Synthesis techniques for BTO preparation include the organo-metallic precursor method, coprecipitation/sol-gel calcination and hydrothermal methods, among others (*Sahoo, et al.* 2007). Some deposition methods are vacuum evaporation, sputtering, laser ablation, hydrothermal synthesis, radio frequency plasma sputtering and sol-gel techniques which have been used for obtaining BTO thin films (*Harizanov, Harizanova and Ivanova* 2004). BTO ceramics can also be processed by techniques such as Spark Plasma Sintering (SPS) (*Buscaglia, et al.* 2004), a change that occurs when cooling through the Curie point, resulting in the involvement of stress-related transformation.

Depending on its crystal structure, BTO can be paraelectric (cubic;  $a=4.031\text{\AA}$ ) or ferroelectric (tetragonal;  $a=3.994\text{\AA}$  and  $c=4.038\text{\AA}$ ) (*Chen, et al.* 2005) (*Maison, et al.* 2001). While low calcination temperatures of ~700°C result in a metastable cubic phase, this can be transformed to tetragonal structures by using higher temperatures, as found by *Maison, et al.* where phase transformation and particle size were analyzed by varying calcination temperature (*Maison, et al.* 2001). It has been demonstrated that chemical homogeneity, material purity, and microstructure have an effect on the positive temperature coefficient of resistivity in BTO. For this reason, methods that provide less contamination, such as coprecipitation, polymerization and sol-gel, are being developed (*Hur, et al.* 1998). For this project, BTO powder was used to fabricate simple geometric figures with a binder jetting technology, the M-Lab system (ExOne, OH). These components were fabricated with different binder saturation percentages and sintered at different temperatures to obtain maximum density. XRD data show no signs of contamination after sintering. Part shrinkage was calculated and used to obtain accurate dimensions for dielectric constant measurements.

### Material, processing, and investigation methods

A total of 500 grams of BTO powder was purchased from Acros Organics through Fisher Scientific. As-received powder can be appreciated in Figure 1. It can be observed

that powder particles are approximately  $1\mu\text{m}$  in diameter, while agglomerations can measure up to  $10\mu\text{m}$ .

Simple geometries of BTO powder were fabricated by the binder jetting process using the ExOne M-Lab system. The basic idea behind this process was to obtain three-dimensional parts bound together in a layer-by-layer fashion. ExOne technologies consist of a two-bed system, shown in the schematic in Figure 2; one is for the base powder material and the other for part fabrication. Powder layers are spread

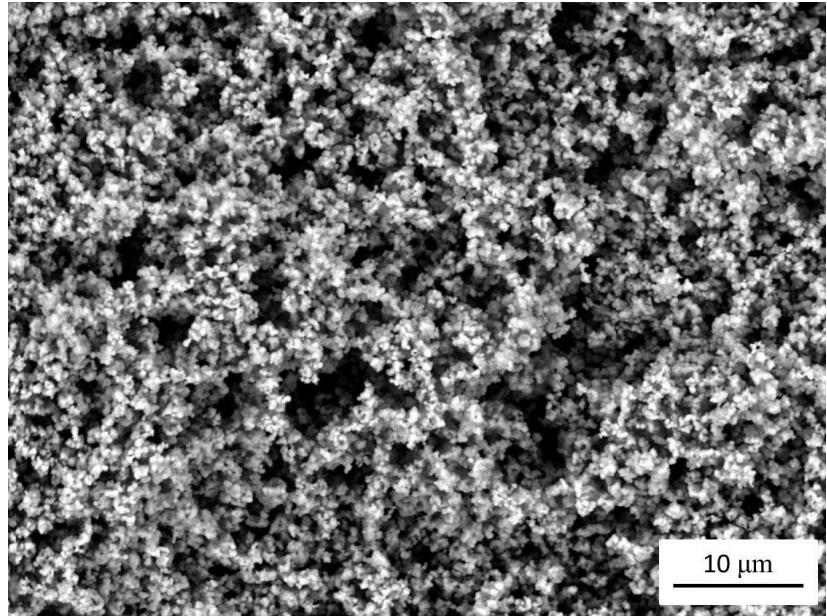


Figure 1. As received BTO powder

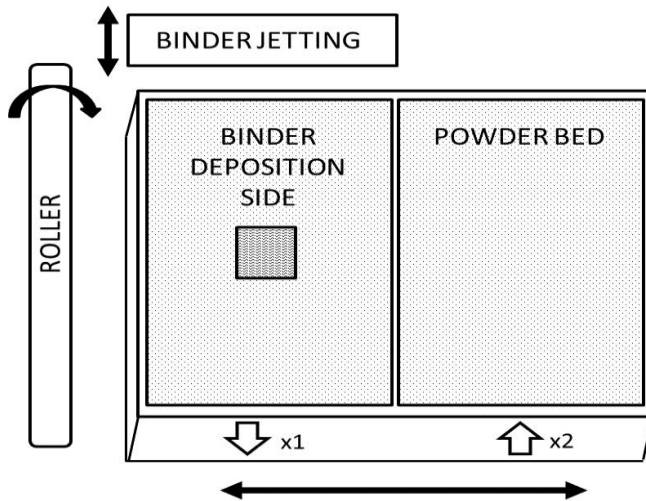


Figure 2. Schematic of powder bed system

with the aid of a roller while the bed is mechanically moving in the x-direction. Once the powder layer is uniformly spread, binder droplets are deposited in the specified places for part fabrication. For this project, a 2:1 ratio of powder and building deposition was used. Fabricated parts, while still in the powder bed, were placed in the oven at  $195^{\circ}\text{C}$  for 2 hours to cure the binder, then cleaned and sintered or infiltrated with a different material. These parts were previously designed by CAD and uploaded into the system as an *.stl* file.

For this project, different building parameters were used and post-sintering density was compared. The binder saturations (which refers to the amount of binder used while building) used were 60, 75, 100 and 120%. Since layer thickness is based on powder size, a  $15\mu\text{m}$  thickness was used at the start of the project. However, since samples were breaking in small pieces after binder curing, the layer thickness was doubled to  $30\mu\text{m}$ , regardless of powder size. Prior to building with a new powder, or even a new layer thickness of the same powder, the M-Lab system requires to calculate and input the powder packing rate before using a new layer thickness.

Two hours at 195°C were used to cure the binder and the samples were cleaned before sintering. A high temperature cyclical furnace (CM, NJ, USA) was used for all sintering temperatures. To simulate non-cyclical furnace cooling profiles, conditions were decided as follows (based on a sintering temperature of  $0.8T_m$ ). Samples were heated at a rate of 10°C/min up to 600°C and held for 0.3 hours, allowing binder burnout. They were then heated up to either 1260°, 1330° or 1400°C, held for four hours, and cooled down to room temperature. Built samples were left inside the furnace until reaching room temperature to avoid faster cooling. Precise temperature profiles are better-represented in Figure 3.

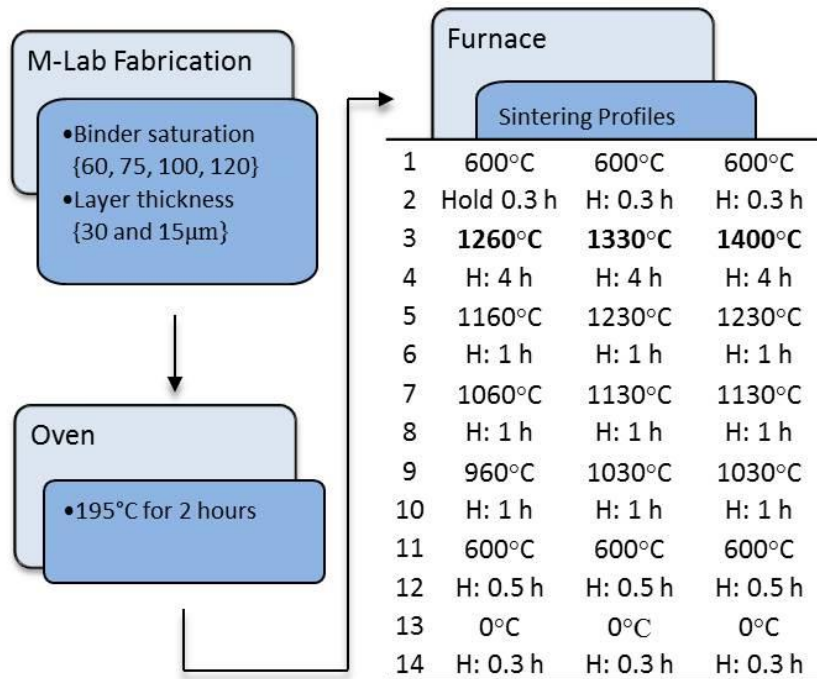


Figure 3. Temperature profiles used to simulate a regular furnace

Density values were obtained by following ASTM B962-08 standard test method (Standards 2009) which uses the Archimedes' principle. A Mettler Toledo MS303S precision scale was used with the aid of a copper mesh to hold the samples in place. A drop of soap was dissolved in the water to reduce surface tension, and olive oil for the immersed samples (used to seal surface porosity and avoid water adsorption), and the water temperature was ~22°C. For this reason we have two types of density, which are referred to as sintered (as removed from the furnace) and impregnated (which were dipped in oil at a pressure of 7kPa for 30 min.). SEM analysis (TM-1000, Hitachi, Japan) was performed using an accelerating voltage of 15kV and no sample preparation was required. XRD analysis was obtained with Cu  $k_\alpha$  radiation (D8, Bruker, Germany). Dielectric constant was obtained with an Agilent Technologies PNA-X Analyzer with a frequency capability of 10MHz to 50GHz.

## Results

With BTO being one of the most versatile ceramics available, the ultimate goal for this project was to obtain dense parts that can provide a dielectric constant comparable to other

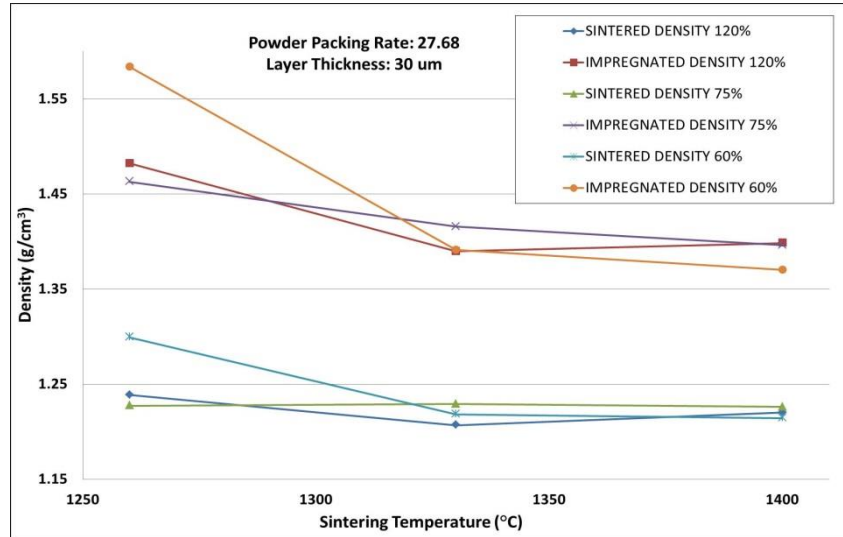


Figure 3. Density vs Sintering Temperature for different binder saturations

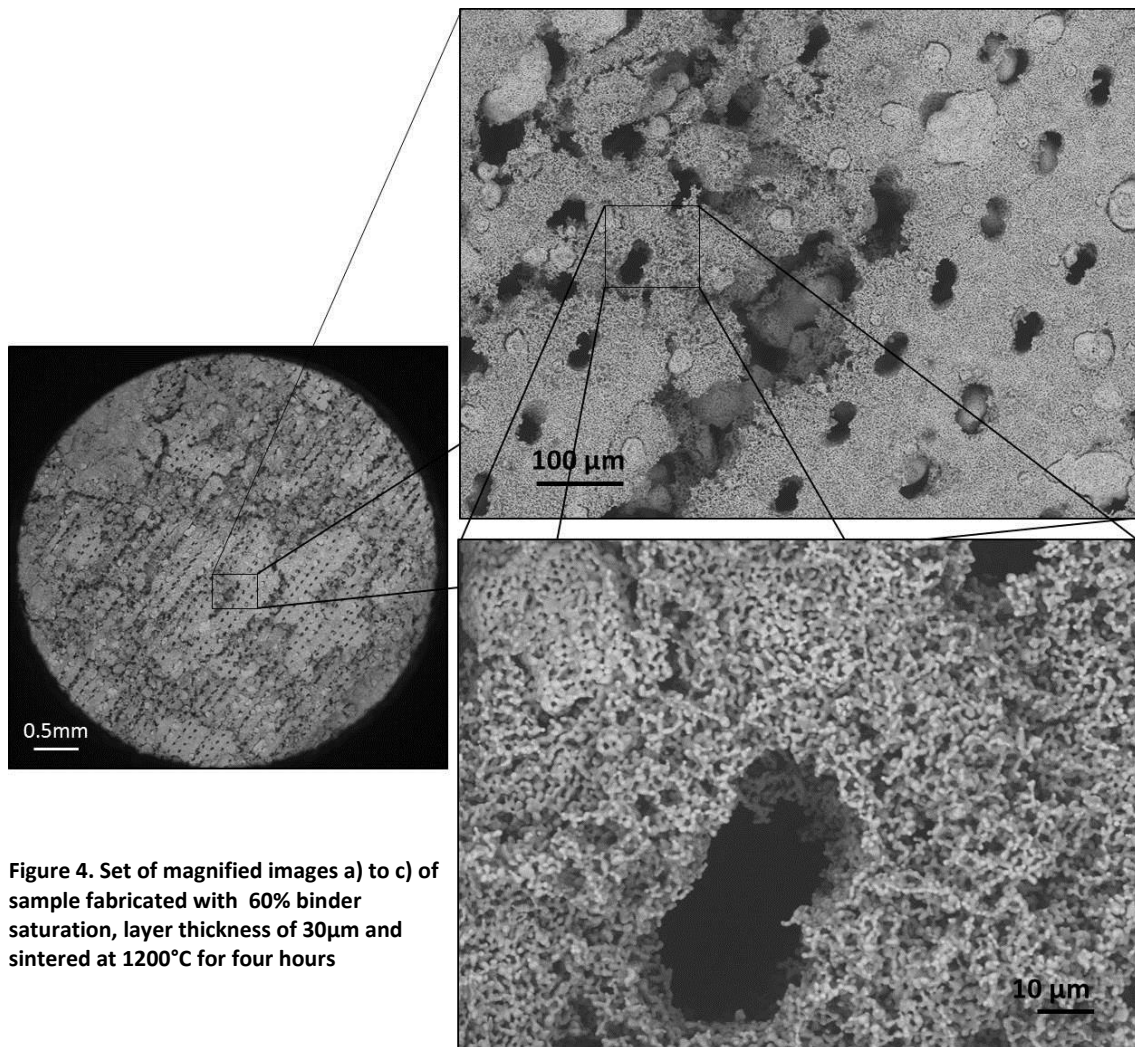


Figure 4. Set of magnified images a) to c) of sample fabricated with 60% binder saturation, layer thickness of 30μm and sintered at 1200°C for four hours

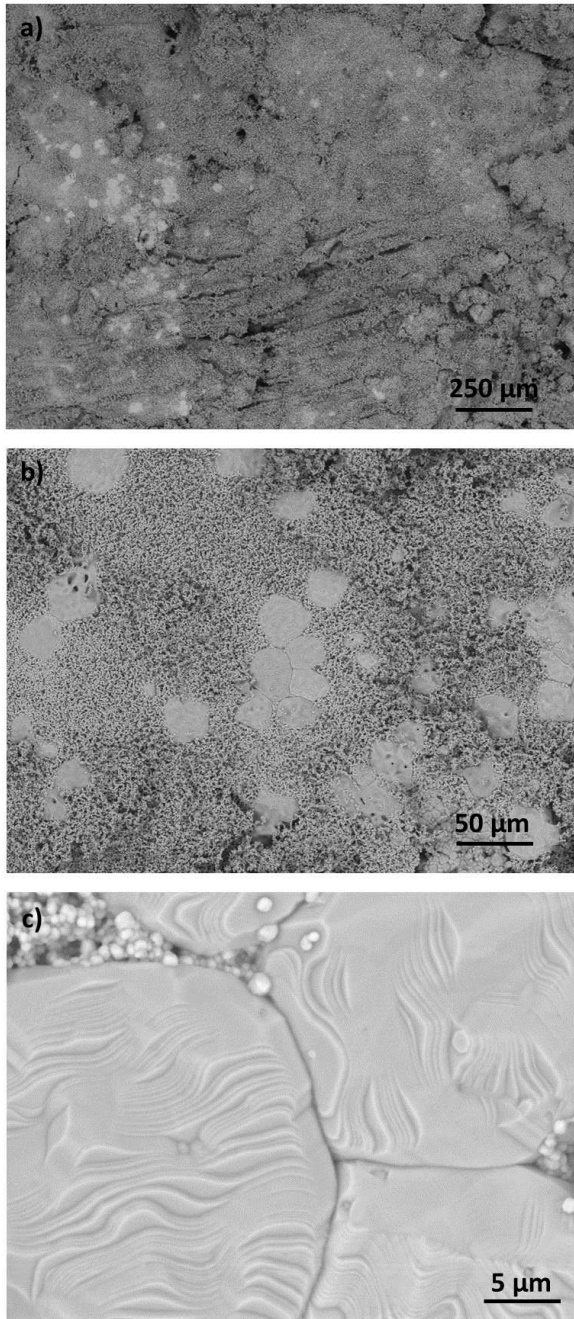


Figure 5. Set of magnified images a) to c) of sample fabricated with 60% binder saturation, layer thickness of 30µm and sintered at 1260°C for four hours.

fabrication methods. Different binder saturations and temperatures were used to fabricate components and density was obtained for those parts. Figure 3 shows the results obtained; each data point depicts the average density of five measured densities. It can be observed that the maximum obtained density value is  $1.6 \text{ g/cm}^3$ , which is about 27% dense for oil impregnated density measurements or  $1.3 \text{ g/cm}^3$  (22% dense) for the sintered part.

Both densities were calculated since it is assumed that the porosity obtained in the parts is interconnected. In addition, unsealed surface porosity absorbs water causing the density values to be higher than the true value. For this reason, it can be observed that two types of density were calculated, sintered and impregnated as observed in Figure 3.

The implied reason for the low density obtained is the lack of pressuring force while sintering. Nonetheless, binder saturation plays an important role in this matter as well. To better understand the process, samples fabricated with 60% binder saturation, which provided the highest density obtained, and a layer thickness of 30µm were sintered at 1200°C for a total of four hours and the surface was analyzed. Figures 4a), b) and c) show a magnified sequence of images where binder has already burned out (process that occurs at  $\sim 600^\circ\text{C}$ ) and empty spaces were left behind. Binder droplets are 60µm in length and 20µm width. This means that BTO grain growth must overcome the empty spaces left behind after binder burnout, and close any gaps around the grains in order to obtain denser parts.

Since the application of force while sintering is not a path to follow for 3D fabricated parts (since complex parts would lose their shape), the temperature was increased to obtain denser parts. According to

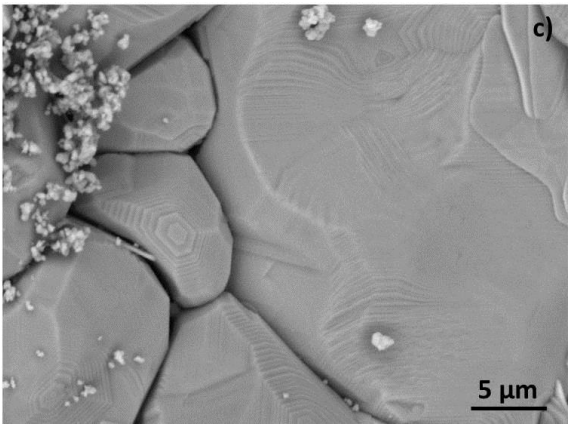
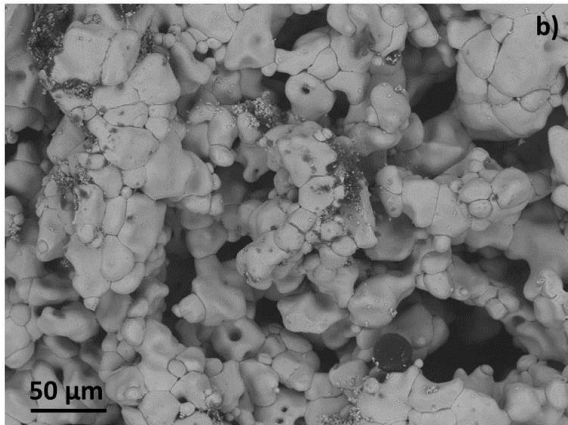
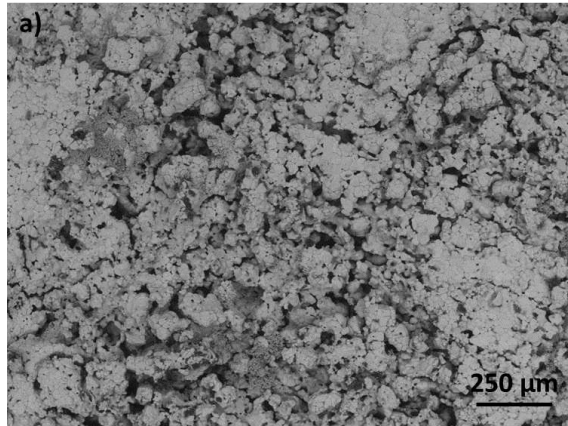


**Figure 6.** Set of magnified images a) to c) of sample fabricated with 60% binder saturation, layer thickness of 30 $\mu$ m and sintered at 1330°C for four hours.

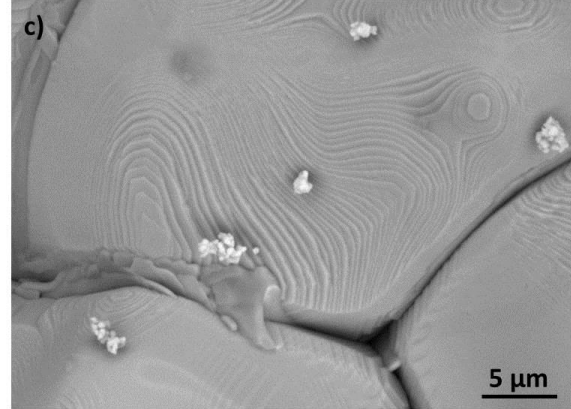
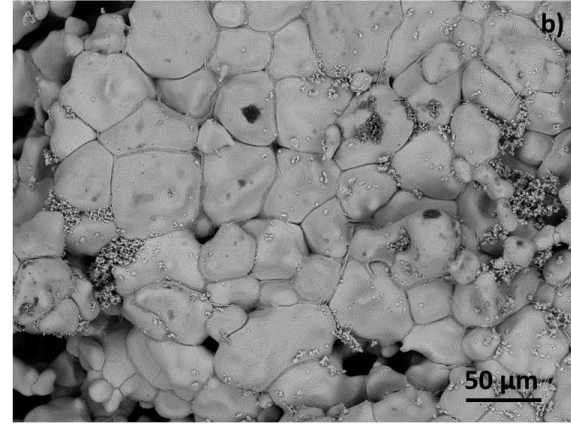
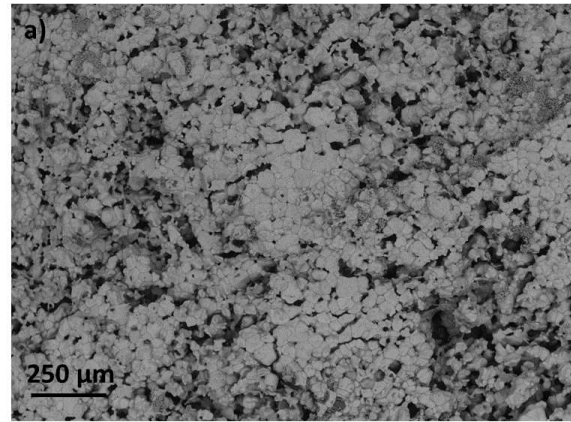


**Figure 7.** Set of magnified images a) to c) of sample fabricated with 60% binder saturation, layer thickness of 30 $\mu$ m and sintered at 1400°C for four hours.

Gao *et al.*, relative density and grain size increased as sintering temperature increased from 1200°C to 1300°C for 2 hours obtaining a density relatively close to 100%. Nonetheless, their powder particle size was 35nm and after powder pressing, sintered samples were only 1 mm in thickness with a maximum grain growth of 2.2  $\mu\text{m}$  (Gao, et al. 2004). In a different study, sintering temperature for powders 30nm in size, consisted of 800°C for ten hours, obtaining a density of more than 90% the theoretical density (Buscaglia, et al. 2004). According to Srinivas, the sintering behavior can be improved by having small, non-agglomerated and equiaxed particles (Subramaniam 2006). For this project, final dimensions consisted of 10.2 x 10.2 x 2.5 mm while starting powder was equiaxed and minimum agglomeration was observed. Nevertheless, density obtained was approximately one fourth of ideal.

Figures 5, 6 and 7, are sequences of images that have been taken at low, medium and high magnifications for samples fabricated with 60% binder saturation and layers of 30 $\mu\text{m}$  in thickness. The difference between each set of images is that samples were sintered at 1260°C, 1330°C and 1400°C, respectively. Given the fact that calculated density for both sintered and impregnated parts provided the highest values obtained for 60% binder saturation, it can be stated that sintered grains attained grain growth. This can be observed in figure 5c) where grain size values range from 25 to 40 $\mu\text{m}$ , and space between grains is fully enclosed. However, Figures 5a) and b) show how most of the powder did not reach any sintering stages and its size remained unchanged. Figures 6 and 7 show less unsintered powder when compared to samples sintered at 1260°C. Images 6 and 7c) show open spaces in between grains, which is not observed in Figure 5c). Densification during sintering can occur mainly in two types of mechanisms, lattice diffusion and grain boundary diffusion, where grain boundaries are the material source for both mechanisms. However, samples sintered at 1330°C and 1400°C show empty spaces in-between the grains when compared to samples sintered at 1260°C. Solid state sintering usually occurs in three stages which are i) initial: involving necking and grain growth, ii) intermediate: resulting in shrinkage and densification, and iii) final: elimination of close pores and formation of dense microstructure (Subramaniam 2006). In our parts, we are probably only reaching the initial stage where grain growth is occurring but it is not uniform. For this reason, further research developing triggering mechanisms for proper sintering behavior of BTO fabricated by the M-Lab system needs to be executed.

Since samples sintered at 1260°C provided the highest density on both sintered and impregnated measurements, our focus converged to those samples. Transition temperatures for BTO from tetragonal crystal structure to cubic is 130°C while transformation from cubic to hexagonal is 1460°C. The issue with obtaining the hexagonal crystal structure is that BTO properties stop being ferroelectric, while tetragonal structures are both polar and ferroelectric (Subramaniam 2006). XRD analysis results showed how the BTO powder obtained is mainly tetragonal with small amounts of cubic phase. After a sintering cycle at 1260°C for four hours, it can be observed how a cubic peak in the 200 direction at  $2\theta=4_{\circ}$  and an hexagonal peak in the 110 direction are observed side-by-side (see Figure 8). According to Chen *et al.*, solid state sintering leads to the cubic phase while cooling, and each grain formed is surrounded by neighboring grains of random orientation closely adhering at the grain boundaries (Chen, et al. 2005), which can explain the tight space between grains in Figure 5. Another study conducted by Gao *et al.*, showed similar results regarding the tetragonal structure's inclination to transform to a cubic phase when sintering BTO powder to 1250°C (Gao, et al. 2004).

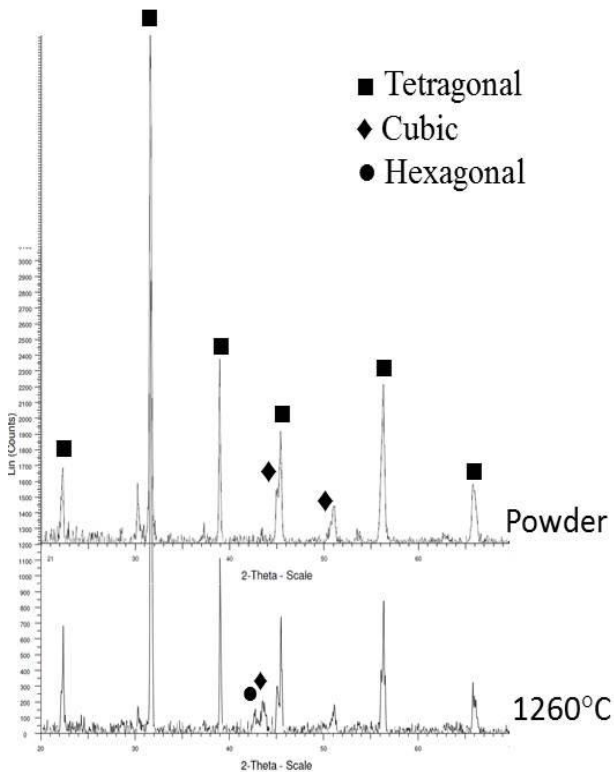


Figure 8. XRD analysis of as-received powder and sample sintered at 1260°C for four hours

To obtain dielectric constant values with a frequency of 12.4 to 18 GHz, samples of 15.8mm in length, 7.9mm in height and 5.08mm in width had to be obtained to use Ku band. For this reason, percent shrinkage was tabulated (Figure 9), and samples were fabricated considering the percent shrinkage obtained after sintering. In addition, CAD files were scaled with  $\pm 1\%$  error to accommodate for any discrepancies during sintering. It was found that samples built taking into consideration the shrinkage percentage calculated did not need any post-processing. On the other hand, samples built to accommodate for the required dimensions that were not scaled before fabrication, required some grinding prior to analysis.

Dielectric constant values ranged from 8.62 to 6.23 for frequencies ranging from 12.4 to 18GHz at room temperature. Results are shown in Figure 10.

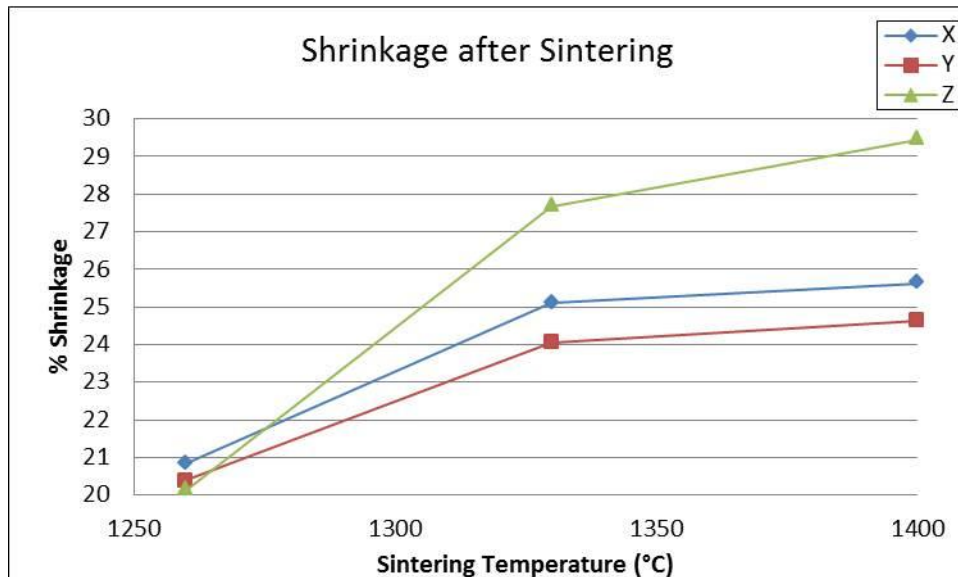


Figure 9. Graph depicting shrinkage percentage in each direction vs sintering temperature

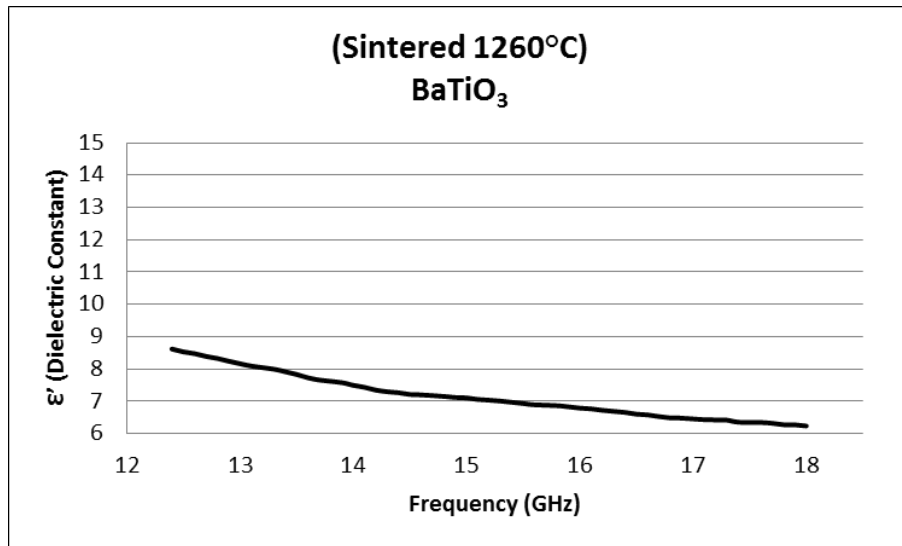


Figure 10. Dielectric constant vs frequency

Applications for multilayer ceramic capacitors imply the importance of accommodating thin dielectric layers and avoid the presence of big particles and pores when designing electronic devices (Chen, et al. 2003)

### Conclusions

BTO promises to be a material that can be fabricated with additive manufacturing. Nonetheless, further research is necessary to obtain optimum properties. From the preliminary results shown in this project the following conclusions can be stated:

- Density after sintering must be increased and future work will include increasing sintering temperature while avoiding grain size growth.
- XRD analysis indicates BTO fabricated by binder jetting technology holds a tetragonal structure even after sintering, providing ferroelectric properties to the ceramic parts obtained.
- Dielectric constant values range from 8.62 to 6.23 as the frequency increases from 12.4 to 18 GHz. Future work consists in further investigation on this value being increased by denser parts, smaller grains and the addition of different coatings.

### Acknowledgements

The research presented here was performed at The University of Texas at El Paso (UTEP) within the W. M. Keck Center for 3D Innovation (Keck Center), expanding recently to over 13,000 sq. ft. and providing access to state-of-the-art facilities and equipment as a result of funding from the State of Texas Emerging Technology Fund. We are also grateful to DOE NETL SC-13-389 for funding this project. Special thanks to Satya K. Gullapalli, Jose Avila, Ubaldo Robles and Maria Yañez.

### References

ASTM Standards, «Standard Test Methods for Density of Compacted or Sintered Powder Metallurgy (PM) Products using Archimedes' Principle.» *Designation: B962 – 08*. PA, USA, 2009.

- Buscaglia, V., y otros. «Nanostructured barium titanate ceramics.» *Powder Technology* 148, 2004: 24-27.
- Chatterjee, Suman, Biljana D. Stojanovic, y H. S. Maiti. «Effect of additives and powder preparation techniques on PTCR properties of barium titanate.» *Materials Chemistry and Physics* 78, 2003: 702-710.
- Chen, J. H., B. H. Hwang, T. C. Hsu, y H. Y. Lu. «Domain switching of barium titanate ceramics induced by surface grinding.» *Materials Chemistry and Physics* 91, 2005: 67-72.
- Chen, R., A. Cui, X. Wang, y L. Li. «Barium titanate coated with magnesium titanate via fused salt method and its dielectric property.» *Materials Science and Engineering B99*, 2003: 302-305.
- Gao, Li Jie, Xiao Lin Liu, Jing Qiang Zhang, Song Quan Wang, y Jian Feng Chen. «Grain-controlled barium titanate ceramics prepared from high-gravity reactive precipitation process powder.» *Materials Chemistry and Physics* 88, 2004: 27-31.
- Harizanov, O., A. Harizanova, y T. Ivanova. «Formation and characterization of sol-gel barium titanate.» *Materials Science and Engineering B106*, 2004: 191-195.
- Hur, S. H., J. K. Lee, K. W. Park, K. S. Hong, y S. J. Park. «Relationship between microstructure and properties of semi-conducting barium titanate prepared by a semi-alkoxide route.» *Materials Letters* 35, 1998: 78-84.
- Maison, W., S. Ananta, T. Tunkasiri, P. Thavornnyutikarn, y S. Phanichphant. «Effect of Calcination Temperature on Phase Transformation and Particle size of Barium Titanate Fine Powders Synthesized by the Catecholate Process.» *ScienceAsia* 27, 2001: 239-243.
- Sahoo, T., S. K. Tripathy, M. Mohapatra, S. Anand, y R. P. Das. «X-ray diffraction and microstructural studies on hydrothermally synthesized cubic barium titanate from TiO<sub>2</sub>-Ba(OH)<sub>2</sub>-H<sub>2</sub>O system.» *Materials Letters* 61, 2007: 1323-1327.
- Subramaniam, S. «In situ high temperature environmental scanning electron microscopic investigations of sintering behavior in barium titanate.» *Dissertation*. University of Cincinnati, 2006.